

The GOME-2
instrument on the
Metop series of
satellites

R. Munro et al.

This discussion paper is/has been under review for the journal Atmospheric Measurement Techniques (AMT). Please refer to the corresponding final paper in AMT if available.

The GOME-2 instrument on the Metop series of satellites: instrument design, calibration, and level 1 data processing – an overview

R. Munro¹, R. Lang¹, D. Klaes¹, G. Poli¹, C. Retscher¹, R. Lindstrot¹, R. Huckle¹, A. Lacan¹, M. Grzegorski¹, A. Holdak¹, A. Kokhanovsky¹, J. Livschitz², and M. Eisinger³

¹EUMETSAT, Eumetsat-Allee 1, Darmstadt, Germany

²European Space Agency – European Space Research & Technology Centre (ESA-ESTEC), Noordwijk, the Netherlands

³European Space Agency – European Centre for Space Applications and Telecommunications (ESA-ECSAT), Didcot, Oxfordshire, UK

Received: 28 April 2015 – Accepted: 15 June 2015 – Published: 11 August 2015

Correspondence to: R. Munro (rosemary.munro@eumetsat.int)

Published by Copernicus Publications on behalf of the European Geosciences Union.

Title Page

Abstract Introduction

Conclusions References

Tables Figures

◀ ▶

◀ ▶

Back Close

Full Screen / Esc

Printer-friendly Version

Interactive Discussion



function characterisation data are available from the GOME-2 monitoring pages in the documentation sub-section at gome.eumetsat.int.

1.4 In-flight characterisation and calibration

A range of in-flight characterisation and calibration activities are carried out routinely during GOME-2 operations. These activities provide input to level 0 to 1b processing, in addition to the calibration key data measured on-ground, to ensure the generation of high quality spectrally and radiometrically calibrated radiance and irradiance data and continuous monitoring of instrument performance.

Calibration activities interleaved with nominal observations comprise dark signal measurements performed every orbit in eclipse and sun calibration measurements performed once per day at sunrise in the Northern Hemisphere. The sun calibration uses one of the on-board stored timelines which includes in addition to the sun measurements itself, both a wavelength calibration and a radiometric calibration. The timeline must be triggered such that the instrument is commanded into SUN observation mode prior to the sun appearing in the instrument field of view. For the remainder of the orbit the timeline consists of nadir scanning observations.

In addition, regular monthly calibration activities take place. The frequency is determined by the expected change in the mean optical bench temperature, resulting from seasonal variations in the external heat load from the sun, and long-term degradation of thermo-optical surfaces. Although it is primarily the wavelength calibration that is expected to vary, diffuser characterisation and other calibration and monitoring activities are carried out during the monthly calibration activities.

The GOME-2 instrument on the Metop series of satellites

R. Munro et al.

Title Page

Abstract

Introduction

Conclusions

References

Tables

Figures



Back

Close

Full Screen / Esc

Printer-friendly Version

Interactive Discussion



1.5 GOME-2 observation modes

1.5.1 Earth observation modes

Earth observation (or “Earthshine”) modes are those modes where the earth is in the field of view of GOME-2. They are usually employed on the dayside of the earth (sunlit part of the orbit). The scan mirror can be at a fixed position (static modes), or scanning around a certain position (scanning modes). All internal light sources are switched off and the solar port of the calibration unit is closed.

- *Nadir scanning*. This is the mode in which GOME-2 is operated most of the time. The scan mirror performs a nadir swath as described above.
- *Nadir static*. The scan mirror is pointing towards nadir. This mode is typically used during the monthly calibration. It is valuable for validation and long-loop sensor performance monitoring purposes.

1.5.2 Calibration modes

In-orbit instrument calibration and characterisation data are acquired in the various calibration modes. They are usually employed during eclipse with the exception of the solar calibration which is performed at sunrise. Both internal (WLS, SLS, LED) and external (sun, moon) light sources can be employed. The various sources are selected by the scan mirror position.

- *Dark*. The scan mirror points towards the GOME-2 telescope. All internal light sources are switched off and the solar port is closed. Dark signals are typically measured every orbit during eclipse.
- *Sun (over diffuser)*. The scan mirror points towards the diffuser. All internal light sources are switched off and the solar port is open. Solar spectra are typically acquired once per day at the terminator in the Northern Hemisphere. The Sun Mean Reference (SMR) spectra are derived from this mode.

The GOME-2 instrument on the Metop series of satellites

R. Munro et al.

Title Page

Abstract

Introduction

Conclusions

References

Tables

Figures



Back

Close

Full Screen / Esc

Printer-friendly Version

Interactive Discussion



The GOME-2 instrument on the Metop series of satellites

R. Munro et al.

Title Page

Abstract

Introduction

Conclusions

References

Tables

Figures

◀

▶

◀

▶

Back

Close

Full Screen / Esc

Printer-friendly Version

Interactive Discussion



- *White light source (direct)*. The scan mirror points towards the WLS output mirror. The WLS is switched on and the solar port is closed. Etalon (and optionally Pixel-to-Pixel Gain (PPG) calibration) data are derived from this mode.
- *Spectral light source (direct)*. The scan mirror points towards the SLS output mirror. The SLS is switched on and the solar port is closed. Wavelength calibration coefficients are derived from this mode.
- *Spectral light source over diffuser*. The scan mirror points towards the diffuser. The SLS is switched on and the solar port is closed. Light from the SLS reaches the scan mirror via the diffuser. This mode is intended to be employed for in-orbit monitoring of the sun diffuser reflectivity. In practise, however, this instrument mode has not been particularly useful as the SLS has proven to be unstable for the long integration times required to measure over the sun diffuser. Analysis of these measurements has only been used to provide a rough estimate of the upper boundary for diffuser degradation.
- *LED*. The scan mirror points towards the GOME-2 telescope. The LEDs are switched on and the solar port is closed. Pixel-to-pixel gain (PPG) calibration data are derived from this mode.
- *Moon*. The scan mirror points towards the moon (typical viewing angles are +70 to +85°). As the spacecraft moves along the orbit, the moon passes the GOME-2 slit within a few minutes. This mode can be employed only if geometrical conditions (lunar azimuth, elevation and pass angle) allow, which typically occur a few times per year.

1.6 GOME-2 instrument operations plan

The default swath width of the scan is 1920 km which enables global coverage of the Earth's surface within 1.5 days. The scan mirror speed can be adjusted such that, despite the projection effect, the ground is scanned at constant speed. The along-track

The GOME-2 instrument on the Metop series of satellites

R. Munro et al.

Title Page

Abstract

Introduction

Conclusions

References

Tables

Figures



Back

Close

Full Screen / Esc

Printer-friendly Version

Interactive Discussion



dimension of the instantaneous field-of-view (IFOV) is ~ 40 km which is matched with the spacecraft velocity such that each scan closely follows the ground coverage of the previous one. The IFOV across-track dimension is ~ 4 km. For the 1920 km swath, the maximum temporal resolution of 187.5 ms for the main channels (23.4 ms for the PMD channels) corresponds to a maximum ground pixel resolution (across track \times along track) of 80 km \times 40 km (10 km \times 40 km for the PMDs) in the forward scan. Since 15 July 2013, both GOME-2 instruments on board Metop-A and Metop-B have been operated in tandem with the swath width of GOME-2 on Metop-A changed to 960 km, while GOME-2 on Metop-B remains with the full swath width of 1920 km. This results in a ground pixel size of 40 km \times 40 km for GOME-2 on Metop-A main science channels (5 km \times 40 km for the PMDs) and 80 km \times 40 km for GOME-2 on Metop-B main science channels (10 km \times 40 km for the PMDs).

The 29 day instrument operations plans for Metop-A and Metop-B are shown in Figs. 2 and 3. The monthly calibration sequence is activated for both instruments on the same day with two nadir static orbits (no scanning) followed by one orbit during which the PMD data is down-linked at full spectral resolution (256 channels for both PMDs) but with a reduced number of readouts (12 read-outs in forward and 4 read-outs in backward scanning direction whilst retaining nominal spatial resolution for PMDs, i.e. with gaps in between the read-outs). This configuration is called the monthly PMD RAW read-out configuration. GOME-2 on Metop-A is also configured to operate once per month with a reduced swath width of 320 km. For further information see the GOME-2 monitoring pages in the timelines sub-section at gome.eumetsat.int. For more details on GOME-2 operations and the instrument settings, see EUMETSAT, 2014a.

1.7 GOME-2 data packet structure and synchronisation of measurements

A basic concept in the operation of the GOME-2 instrument is that of the “scan”. A scan is defined as a time interval of 6 s, consisting of 16 “subsets” of 375 ms each, equivalent to one data packet. The subsets are numbered from 0 to 15. In the earth scanning mode, a scan consists of one scan cycle: 4.5 s forward scan (subsets 0 to 11) and 1.5 s

fly-back (subsets 12 to 15). In the static and calibration modes the scan mirror does not move, but the data packet structure is identical to the scanning mode.

In the default measuring mode, the nadir scan, the scan mirror sweeps in 4.5 s (12 subsets) from negative (East) to positive (West) viewing angles, followed by a fly-back of 1.5 s (the last 4 subsets) back to negative viewing angles as shown in Fig. 4.

GOME-2 creates a Science Data Packet every 375 ms. One packet contains one UTC time stamp t_0 , four scanner positions (sampling 93.75 ms), at most two readouts of the main channels (effective integration time 187.5 ms), at most 16 readouts of the PMD bands (integration time 23.4375 ms).

Their relative timing is shown in Fig. 5. The first scanner position is given at time $t_0 + \Delta t_{SM}$ (the time delta for the scan mirror between one data packet and the next). At the same time, the first main channel readout and the first PMD readout within the packet start. The readout time is 45.78 μ s for one detector pixel, i.e. 46.875 ms for a complete main channel readout (1024 detector pixels), and 11.72 ms for a readout of PMD blocks BCD (256 detector pixels, see EUMETSAT, 2014a.). Any readout operation resets a detector pixel, and therefore marks the *end* of the integration for this detector pixel. The integration starts at the *previous* readout.

The readout sequence for each detector can be programmed to be either from short to long wavelengths (“up”) or from long to short wavelengths (“down”).

2 GOME-2 Level 0 to 1 data processing

GOME-2 data level 0 data are processed centrally at EUMETSAT in near-real time and made available to users through a variety of mechanisms. More information on data access can be found at www.eumetsat.int > Data > Data Delivery. The data processing is separated into two main stages level 0 to 1a processing and level 1a to 1b processing.

The GOME-2 instrument on the Metop series of satellites

R. Munro et al.

Title Page

Abstract

Introduction

Conclusions

References

Tables

Figures



Back

Close

Full Screen / Esc

Printer-friendly Version

Interactive Discussion



2.1 Level 0 to 1a processing

The level 0 to 1a processing comprises both the determination of geolocation information on a fixed time grid, and the determination of applicable calibration parameters. From measurements of the various calibration sources encountered during each run of the processor, new calibration constants are calculated and written into an in-flight calibration data file. They are also retained in memory for use in processing those data acquired after the satellite comes out of the dark side of the orbit and before the next dump. Updated calibration parameters are available for immediate use. Calibration parameters are stored for the lifetime of the mission. The calibration constant determination comprises:

- dark current correction
- pixel-to-pixel gain correction
- determination of spectral calibration parameters
- etalon correction
- determination of stray light correction factors for the sun and polarisation measurements
- determination of the solar mean reference spectrum, and atmospheric polarisation state

The geolocation of the measurements is calculated from the appropriate orbit and attitude information, and time correlation information in the level 0 data stream. Note, any application of calibration parameters in the level 0 to 1a processing should be regarded as interim, to facilitate the generation of new calibration parameters and correction factors. There is no application of calibration parameters to main channel earth observation measurements. The output of the level 0 to 1a processor is formatted into the level 0 and 1a products as specified in EUMETSAT, 2010 and 2014d.

The GOME-2 instrument on the Metop series of satellites

R. Munro et al.

Title Page

Abstract

Introduction

Conclusions

References

Tables

Figures



Back

Close

Full Screen / Esc

Printer-friendly Version

Interactive Discussion



2.2 Level 1a to 1b processing

The level 0 to 1b processing comprises the calculation of geolocation parameters for the actual integration time of each measurement, determination of stray light correction factors for the Earthshine measurements, and the conversion of the raw binary readouts on the level 1a data stream to calibrated radiance and irradiance data. Cloud parameters are also determined. Furthermore, calibrated measurements from the on-board calibration sources, and the sun and moon are available in the level 1b product. Level 1b data are formatted as specified in EUMETSAT, 2010 and 2014d.

3 GOME-2 Level 0 to 1 Algorithms

3.1 Geolocation and synchronisation of main channel and PMD data

Basic geolocation parameters such as the sub-satellite point and solar angles at the satellite are calculated for all measurement modes. In addition, mode-specific geolocation parameters are calculated for earth, sun, and moon modes as follows:

- *Earth mode.* Solar and line-of-sight zenith and azimuth angles at a given height, corner and centre coordinates (latitude/longitude) of the ground pixel at ground level, satellite height, and earth radius.
- *Sun mode.* Distance between satellite and sun and relative speed of satellite and sun.
- *Moon mode.* Lunar elevation and azimuth angles, sun-moon distance, satellite-moon distance, lunar phase angle, illuminated fraction of lunar disk.

Geo-location parameters are processed during level 0 to 1b processing both for a fixed grid of 32 read-outs per scan and for an individual grid based on the actual integration time of an instrument band. Figure 6 shows the orientation of the GOME-2 ground pixel within the scan and relative to the flight direction. Letters A-F indicate

The GOME-2 instrument on the Metop series of satellites

R. Munro et al.

Title Page

Abstract

Introduction

Conclusions

References

Tables

Figures



Back

Close

Full Screen / Esc

Printer-friendly Version

Interactive Discussion



the position, relative to the ground pixel, of points for which geolocation information is provided in the GOME-2 level 1b product.

Note that geolocation information is provided in the GOME-2 level 1b product only for the first detector pixel of each channel (EUMETSAT, 2010 and 2014d). Therefore for a proper assignment of geolocation to the GOME-2 measurements and for a correct combination of main channel and PMD data, the synchronisation of UTC time stamps, scan mirror positions and detector readouts in the science data packet have to be understood, and the relative timing of the main channel and PMD readouts, and the finite duration of the detector readouts, must be accounted for.

Specifically, the user of the geolocation information needs to be aware that the so-called effect of “spatial aliasing” has to be accounted for when very accurate georeferencing or co-registration of main channel and PMD data is needed. The “spatial aliasing” effect arises because the individual detector pixels are read out sequentially whilst the scan mirror is still moving. As a result every detector pixel of each detector sees a slightly different ground scene and thus spatial information is “aliased” into spectral information. The detector arrays have been programmed to read out in alternating direction so that the last and first detector pixels of spectrally adjacent channels see approximately the same scene thus minimising discontinuities between channels. The readout direction is specified in the field CHANNEL_READOUT_SEQ of GIADR-Channels record in the GOME-2 level 1b product (EUMETSAT, 2010 and 2014d).

Knowing the time taken to read out a single detector pixel $\delta_{rd} = 45.78 \mu\text{s}$ it is possible to calculate the time taken from the readout of the first detector pixel, for which geolocation information is provided, to the readout of the detector pixel of interest and thereby calculate accurate timing and geolocation information for the pixel of interest.

For detector pixel i of channel j of the main science channels, the time delay is calculated as:

$$t_{ij,FPA} = \begin{cases} i \times \delta_{rd}(\text{readout sequence “up”}) \\ (1023 - i) \times \delta_{rd}(\text{readout sequence “down”}) \end{cases} \quad (1)$$

**The GOME-2
instrument on the
Metop series of
satellites**

R. Munro et al.

Title Page	
Abstract	Introduction
Conclusions	References
Tables	Figures
◀	▶
◀	▶
Back	Close
Full Screen / Esc	
Printer-friendly Version	
Interactive Discussion	



and for detector pixel k of the two polarisation detectors, the time delay is calculated as:

$$t_{k,\text{PMD}} = \begin{cases} (k - 768) \times \delta_{\text{rd}}(\text{readout sequence "up"}) \\ (1023 - k) \times \delta_{\text{rd}}(\text{readout sequence "down"}) \end{cases} \quad (2)$$

To calculate the shift in geolocation parameters resulting from this time delay related to detector readout, a simple linear interpolation between the geolocation parameters provided for the first detector pixel of readout n and readout $n + 1$ is sufficient.

So for main science channel data

$$\text{geolocation}_{i,\text{actual}} = \frac{t_{ij,\text{FPA}}}{IT_{\text{FPA}}} \times (\text{geolocation}_{n+1} - \text{geolocation}_n) + \text{geolocation}_n \quad (3)$$

and for polarisation channel data

$$\text{geolocation}_{k,\text{actual}} = \frac{t_{k,\text{PMD}}}{IT_{\text{PMD}}} \times (\text{geolocation}_{n+1} - \text{geolocation}_n) + \text{geolocation}_n \quad (4)$$

Where IT_{FPA} and IT_{PMD} are the integration times in use for the main channels and PMDs respectively, which determine the time difference between successive readouts for which geolocation information of the first detector pixel is available.

In case the user wishes to co-register main channel and PMD data care must also be taken to account for the synchronisation between the measurements as shown in Fig. 5 so that the main channel and PMD data correspond as closely as possible to the same ground scene. This is needed for example when PMD data are co-registered with main channel data for the derivation of the polarisation correction, or when co-registering cloud information provided at PMD resolution (see Sect. 3.9) with main channel data. Here the relative timing between the readout of a main channel detector pixel and the readout of a PMD-Pixel at the same wavelength must be considered. This is determined by the readout time per detector pixel, the readout sequence of the

The GOME-2 instrument on the Metop series of satellites

R. Munro et al.

Title Page

Abstract

Introduction

Conclusions

References

Tables

Figures

◀

▶

◀

▶

Back

Close

Full Screen / Esc

Printer-friendly Version

Interactive Discussion



GOME-2 channels (“up” or “down”), and their dispersion relation (pixel – wavelength correspondence), see Fig. 7.

First it is necessary to create four sets of eight averaged PMD readouts (\bar{p}_m where $m = 0 \dots 3$) for each main 187.5 ms channel readout, each shifted by one PMD readout (23.4 ms) with respect to each previous set. See Fig. 5 for a graphical representation in the case of use of PMD data for polarisation correction and also Fig. 7.

Using the PMD wavelength grid, the PMD detector pixel k which is closest in wavelength to the main channel wavelength λ_{ij} for detector pixel i of channel j of the main science channels, is determined. Each main channel detector pixel is then assigned a parameter m^r expressing its timing relative to the timing of the PMD data for $m = 0$ calculated as:

$$m_{ij}^r = (t_{ij,\text{FPA}} - t_{k,\text{PMD}}) / 23.4375 \text{ ms} + 1 \quad (5)$$

where 23.4375 ms is the integration time of a single PMD measurement. The start of the main channel readout is chosen as the time origin ($t = 0$). This corresponds to the start of the last readout of the PMD channels which have been averaged into set $m = 1$ (see Fig. 7). For example, if a pixel has $m^r = 1.6$ (highlighted in Fig. 7) it would correspond to a measurement 0.6 ms \times 23.4 ms later than the PMD data from set $m = 1$, and 0.4 ms \times 23.4 ms before the PMD data from set $m = 2$.

If m^r is split into its integer part $m^{r,\text{int}}$ and its fractional part $m^{r,\text{frac}}$ using a modulus function, the four sets (\bar{p}_m where $m = 0 \dots 3$) of averaged PMD information can be reduced to a single set p_s , taking into account the relative timing between main channels and PMD channels, by calculating:

$$p_{s,ij} = \left(1 - m_{ij}^{r,\text{frac}}\right) \cdot \bar{p}_{ij,m} + m_{ij}^{r,\text{frac}} \cdot \bar{p}_{ij,m+1} \quad \text{where } m = m_{ij}^{r,\text{int}}. \quad (6)$$

3.2 Dark signal correction

The dark signal for each combination of integration time and detector temperature is calculated as an average of measurements taken in dark mode during eclipse. Applying

The GOME-2
instrument on the
Metop series of
satellites

R. Munro et al.

Title Page

Abstract

Introduction

Conclusions

References

Tables

Figures



Back

Close

Full Screen / Esc

Printer-friendly Version

Interactive Discussion



spectrum. The PPG correction is of the order of 10^{-4} relative with some increases for channel 1 and 2 towards the end of the time period for Metop-A. The contribution of this signal to the overall throughput degradation and variation of calibrated radiances is however small.

3.4 Spectral calibration and instrument spectral response function

Spectral calibration is the assignment of a wavelength value to each detector pixel. For each GOME-2 channel, a low order polynomial approximation is used to describe wavelength as a function of detector pixel. Polynomial coefficients are derived from pre-processed spectra of the on-board SLS which provides a number of spectral lines at known wavelengths across the GOME-2 wavelength range. Different algorithms are used for FPA and PMD channels because their spectral resolution is different. Individual spectral lines can only be resolved in the FPA channels. Positions of individual lines from a predefined set are determined using a Falk centre-of-gravity algorithm. For the PMD channels an iterative cross-correlation algorithm is used. The expected PMD-Signal is calculated from the measured FPA signal, taking into account the PMD-Slit function and ratio of radiometric response between PMD and FPA channels. The expected PMD-Signal is then spectrally matched with the measured PMD-Signal using cross-correlation.

The detector pixel onto which light of a given wavelength is impinging depends on instrument temperature. The temperature at the pre-disperser prism is used as a reference. Typical shifts with temperature are of the order of $0.01 \text{ detector pixel K}^{-1}$ for the FPA channels, but depend on detector pixel.

Currently one spectral calibration is carried out on board every day. Spectral stability in orbit, which is a function of pre-disperser prism temperature, is very good. However, there is a very well known orbital variation in spectral assignment due to the orbital change of the optical bench temperature which is not thermally stabilised. Also, there

The GOME-2 instrument on the Metop series of satellites

R. Munro et al.

Title Page

Abstract

Introduction

Conclusions

References

Tables

Figures



Back

Close

Full Screen / Esc

Printer-friendly Version

Interactive Discussion



However, it has been observed that this is not the case and that the change in FWHM follows two patterns.

First, a spectrally well ordered pattern (see Fig. 9) during which the FWHM continuously decreases especially for the lower wavelength range. A similar pattern has been observed in the solar Fraunhofer lines by users of level 1 data. This long-term change is anti-correlated with the long-term trends in the optical bench temperature of the instrument (see Fig. 10).

Second, the FWHM varies significantly with the seasonal in-orbit change in the thermal environment. This can easily be verified when comparing the seasonal signals with the optical bench temperature provided in Fig. 10. The seasonal signal of FWHM changes is correlated with the optical bench temperature for channel 1, 3 and 4, while in channel 2 is anti-correlated.

3.5 Etalon correction

Interference in the thin detector coating layer causes a wave-like pattern on the radiance response (fixed etalon). When deposits settle on the detector coating, the interference pattern is changed (variable etalon). The etalon correction accounts for changes in the variable etalon between on-ground calibration (reference etalon) and the in-orbit situation. It is calculated from daily pre-processed spectra of the on-board WLS. The in-orbit WLS spectrum is nominally ratioed to a reference WLS spectrum representative of the on-ground calibration of the radiance response. The WLS spectra measured in-orbit show an expected characteristic baseline shift as compared to on-ground measurements, which is removed in the data processing. For each channel, a band-pass filter is applied to the ratio. Spectral components within the band-pass (typically 4–10 oscillations per channel) are declared to be the etalon correction. Etalon correction typically is of the order of 10^{-2} relative. The remainder is called etalon residual. Applying the etalon correction means dividing a spectrum by the etalon correction spectrum.

As the basis for the etalon correction is a baseline removed ratio of the on-ground reference WLS to the in-orbit lamp measurements there is an implicit assumption that

The GOME-2 instrument on the Metop series of satellites

R. Munro et al.

Title Page

Abstract

Introduction

Conclusions

References

Tables

Figures



Back

Close

Full Screen / Esc

Printer-friendly Version

Interactive Discussion



The GOME-2 instrument on the Metop series of satellites

R. Munro et al.

Title Page

Abstract

Introduction

Conclusions

References

Tables

Figures



Back

Close

Full Screen / Esc

Printer-friendly Version

Interactive Discussion



5 tio of calibrated PMD-P to PMD-S signals for this un-polarised light are expected to be one. Any deviation reflects a change in the relative radiometric response of the PMDs. By accumulating data for these special geometries over time, to minimise noise, a correction to the relative radiometric response of the PMDs is derived and subsequently
 10 used in the data processing. The update frequency depends on the quality of the accumulated data and the derived correction and is typically between 4 and 7 days. For more details see EUMETSAT, 2014b. Subsequent analysis of the calculated q Stokes fractions including application of the online correction, derived from the special geometry conditions described above, serves as a check for the overall consistency of the
 15 polarisation correction and shows very small deviations (less than 0.02) from zero over the whole time period of the mission.

In order to monitor and validate the measured GOME-2 Stokes fractions for conditions other than the special geometry conditions, a more general approach is needed. The approach used is based on a statistical analysis developed by SRON under contract to ESA (Tilstra, 2008). It can be shown that the general behaviour of the Stokes
 20 fraction, q , along the orbit is primarily determined by molecular (Rayleigh) scattering, in particular over dark ocean surfaces, and that variability in q is caused by the presence of clouds and aerosols. It is observed that the measured polarisation values are always clearly between extreme limiting values. These limiting values lie between the Rayleigh
 25 single scattering values and $q = 0$. Furthermore, for a large number of measurements the measured polarisation values are influenced by largely cloudy scenes which depolarise the light leading to a measured Stokes fraction of $q = 0$. The assumption, upon which the generalised validation of q is based, is that the minimum Stokes fractions observed are representative of a limiting atmosphere with minimum depolarisation, i.e. a combination of minimum ground albedo and minimum aerosol loading. In the case
 of little or no instrument degradation these limiting values will be constant in time and can be used as an empirical validation method for the long-term in-flight monitoring of polarisation measurements. Figure 12 shows Stokes fractions calculated from Earthshine scanning measurements as compared to the single scattering Stokes fractions

(diagonal line) and $q = 0$. Red points lie inside the physically reasonable range while blue points lie outside the physically reasonable range.

The “limiting atmosphere” plots for q Stokes fraction values are derived for all PMD band values and for one orbit in 2009 (Fig. 12). From the absence of outliers we conclude that the quality of the Stokes fractions and their stability is very good based both on the “limiting atmospheres” and special geometries analysis. See also Tilstra et al., 2014 for an independent analysis.

3.8 Stray light correction

Spectral stray light is (unwanted) light from wavelengths other than the nominal wavelength measured by a given detector pixel. Two types of stray light can be distinguished – uniform and ghost stray light. Uniform stray light originates in diffuse scatter inside the instrument and generates a slowly varying or nearly uniform stray light across a detector array and ghost stray light originates in specular reflection from optical components within the instrument. For each ground pixel the uniform stray light contribution is calculated by weighting the sum of the measured signals in a channel with the corresponding stray light fraction from the calibration key data. The ghost stray light position and intensity is calculated from the “parent” position and intensity using polynomial coefficients from the key data. Both types have been characterised during on-ground calibration from which it is clear that the most important component is the uniform stray light, particularly in channel 1. Applying the stray light correction means subtracting the total stray light (sum of uniform and ghost stray light) from the measured signals. The stray light correction is typically smaller than 10^{-3} relative.

The stray light correction applied during the level 0 to 1 processing uses stray light characterisation as delivered following the on-ground calibration and characterisation activities. However, several users of the level 1 data have indicated that during retrieval of geophysical products, increasing fit-residual biases have been observed (particularly in channel one and increasing with decreasing wavelength) which may be due to increasing stray light levels (Cai et al., 2012). This is currently under investigation.

The GOME-2 instrument on the Metop series of satellites

R. Munro et al.

Title Page

Abstract

Introduction

Conclusions

References

Tables

Figures



Back

Close

Full Screen / Esc

Printer-friendly Version

Interactive Discussion



3.9 Calculation of cloud parameters

An effective cloud fraction and cloud top pressure are retrieved for each GOME-2 ground pixel using the Fast Retrieval Scheme for Clouds from the Oxygen A band (FRESCO+) developed by KNMI (Wang et al., 2008). The FRESCO+ retrieval method is based on a comparison of measured and simulated reflectivities in three approximately 1 nm wide spectral windows in and around the oxygen A band (758, 761, 765 nm). Information on cloud fraction mainly comes from the continuum (high intensity for high cloud cover). Information on cloud top pressure mainly comes from the oxygen A band itself (high absorption for low cloud). For a detailed validation of the FRESCO+ output in the level 1b product we refer to Tuinder et al., 2011.

Additional cloud information, based on the AVHRR cloud mask, is also provided in the GOME-2 level 1b product. This comprises geometric cloud fraction and scene homogeneity information derived from AVHRR cloud information and radiance measurements, on a fixed PMD read-out grid of 256 read-outs per scan. Note that in order to use the AVHRR cloud information provided at PMD resolution, for derivation of geophysical products at main channel resolution, it is necessary to carefully account for the synchronisation of main channel and PMD data as described in Sect. 3.1. For further information on the AVHRR derived cloud information please see EUMETSAT, 2014e.

Cloud parameters derived both using the FRESCO+ algorithm and from AVHRR data are reported in the GOME-2 level 1b products for use in higher level processing (EUMETSAT, 2010 and 2014d). They are not used any further in the level 0 to 1 processor.

Figure 13 shows an example of the main channel cloud fraction values from the operational Metop-A FRESCO+ product at 40 km × 40 km main channel spatial resolution in comparison to the AVHRR derived geometric cloud fraction at PMD resolution (5 km × 40 km). In addition the FRESCO+ cloud top height (at main channel resolution) and the AVHRR derived scene homogeneity (at PMD resolution) are also presented.

AMTD

8, 8645–8700, 2015

The GOME-2 instrument on the Metop series of satellites

R. Munro et al.

Title Page

Abstract

Introduction

Conclusions

References

Tables

Figures

◀

▶

◀

▶

Back

Close

Full Screen / Esc

Printer-friendly Version

Interactive Discussion



The GOME-2 instrument on the Metop series of satellites

R. Munro et al.

Title Page

Abstract

Introduction

Conclusions

References

Tables

Figures



Back

Close

Full Screen / Esc

Printer-friendly Version

Interactive Discussion



The results show the fundamental difference between radiometric cloud fraction values (FRESCO+) and geometric cloud fraction values as derived from AVHRR imager data. Optically thin clouds have significantly less impact or are not accounted for at all in radiometric cloud fraction as, for the radiometric cloud fraction, there is a strong relation between optical thickness and cloud fraction. The geometric cloud fraction is however much more sensitive to the presence of a cloud. Please note however, that depending on the application and the radiative transfer model used for a given geophysical parameter retrieval, the radiometric cloud fraction could be the more appropriate choice since not all retrieval algorithms rely on an accurate and very strict cloud screening. The ones that do may favour the geometric cloud fraction instead. For more details on this issue we refer to Loyola et al., 2007; Tuinder et al., 2011, and EUMETSAT, 2014e.

3.10 Application of radiance response

Absolutely calibrated radiances in physical units [$\text{photons}(\text{s cm}^2 \text{ nm sr})^{-1}$] are calculated from pre-processed signals in instrument units [BU s^{-1}]. This is done by dividing the pre-processed signals by the radiance response MME for the actual scanner viewing angle.

Radiances are strongly dependent on observation geometry and ground scene. Even for a fixed geometry a variation of one order of magnitude between a cloudy and a cloud-free scene is common. For a solar zenith angle of 60° , typical radiance values are between 10^{13} and 10^{14} $\text{photons}(\text{s cm}^2 \text{ nm sr})^{-1}$ in the visible to near-infrared.

The point where the radiometric response of the instrument is equal for two physically separate detector arrays (channels) is called the “overlap point” between channels. The spectra per channel are usually cut at this overlap point and concatenated when radiances are to be used from spectral regions bridging a channel separation. This commonly happens for the channel 1 and 2 overlap point around 311 nm. Many level 2 retrievals involving ozone and SO_2 use radiances from both above and below this separation point. In addition, many radiometric corrections evaluated in this region are carried out only within the spectral region defined by the overlap points between

provide relatively stable conditions during the year and from year to year in order to minimize the effect of seasonality, pollution events, and local climate changes. This analysis also shows similar loss of throughput.

Degradation in GOME-2 most likely has two origins: contamination of the primary scan mirror, the most exposed optical element, which was expected based on GOME/ERS-2 experience; and contamination in the region of the detectors themselves which has not been observed with GOME/ERS-2. The degradation may have different characteristics for different optical paths (e.g. Earth, Sun, WLS etc) depending on the optical components involved. For example analysis of the SLS over diffuser measurements, despite the measurements being very unstable (see Sect. 1.5.2), indicates an upper boundary for diffuser degradation of less than 10% over seven years in orbit. In contrast the initial analysis of the differential degradation between the solar and Earthshine measurements suggests a higher rate of degradation at the lowest wavelengths which may be due to the primary mirror at the sun-port entrance (see inlay A of Fig. 1). Loss of signal necessarily decreases signal to noise ratios. Degradation of mirror surfaces may also affect the polarisation response leading to an angular dependence in degradation effects (Krijger et al., 2014). Additionally, changes in the characteristics of the diffuser used to view the sun or features in the level 1b data arising from the diffuser can lead to artefacts in the level 2 data products (EUMETSAT, 2011).

Degradation of the GOME-2 instrument on Metop-B has also been observed and is similar but not exactly the same as that observed for GOME-2 on Metop-A with a slightly lower degradation rate in channel 2 (EUMETSAT, 2015a, b).

The analysis of the GOME-2 degradation is on-going for all operational instruments with the aim of characterising the degradation in reflectivity, in spectral, angular and temporal space, in order to provide a degradation correction to users. Note however that signal to noise cannot be recovered. The degradation analysis and correction will be the subject of a dedicated publication.

The GOME-2 instrument on the Metop series of satellites

R. Munro et al.

Title Page

Abstract

Introduction

Conclusions

References

Tables

Figures



Back

Close

Full Screen / Esc

Printer-friendly Version

Interactive Discussion



5 Conclusions

The GOME-2 instrument, which flies on the Metop-series of satellites, the first of which was launched on 19 October 2006, senses the Earth's backscattered radiance and extraterrestrial solar irradiance in the ultraviolet and visible part of the spectrum. Extensive on-ground calibration and characterisation, and in-orbit calibration activities have guaranteed the provision of high quality calibrated level 1 data which are provided to users in near-real time. On-going monitoring and analysis activities guarantee the continued high quality of the level 1 data. Instrument degradation causing loss of throughput in the instruments is the subject of an on-going analysis which will result in a correction to be provided to users. This analysis will be the subject of a separate publication.

Acknowledgements. The authors would like to acknowledge the work of the large team of colleagues at EUMETSAT, ESA, and in industry, and including our scientific partners, that have contributed to the success of the whole EUMETSAT Polar System, and in particular the GOME-2 instrument.

References

- Callies, J., Corpaccioli, E., Eisinger, M., Hahne, A., and Lefebvre, A.: GOME-2 – Metop's second-generation sensor for operational ozone monitoring, *ESA Bull.-Eur. Space*, 102, 28–36, 2000.
- Cai, Z., Liu, Y., Liu, X., Chance, K., Nowlan, C. R., Lang, R., Munro, R., and Suleiman, R.: Characterization and correction of Global Ozone Monitoring Experiment 2 ultraviolet measurements and application to ozone profile retrievals, *J. Geophys. Res.*, 117, D07305, doi:10.1029/2011JD017096, 2012.
- EUMETSAT: GOME-2 L1 Product Format Specification, EUMETSAT, Darmstadt, Germany, EPS.MIS.SPE.97232, v9, 74 pp., 2010.
- EUMETSAT: Investigation on GOME-2 Throughput Degradation, EUMETSAT, Darmstadt, Germany, EUM/LEO/REP/09/0732, Issue 1.1, 58 pp., 2011.

The GOME-2 instrument on the Metop series of satellites

R. Munro et al.

Title Page

Abstract

Introduction

Conclusions

References

Tables

Figures



Back

Close

Full Screen / Esc

Printer-friendly Version

Interactive Discussion



The GOME-2 instrument on the Metop series of satellites

R. Munro et al.

Title Page

Abstract

Introduction

Conclusions

References

Tables

Figures



Back

Close

Full Screen / Esc

Printer-friendly Version

Interactive Discussion



EUMETSAT: GOME-2/Metop-A Level 1B Product Validation Report No. 5: Status at Reprocessing, EUMETSAT, Darmstadt, Germany, G2RP-R2, EUM/OPS/EPS/REP/09/0619, v1F, 110 pp., 2012.

EUMETSAT: EPS Metop-B Product Validation Report: GOME-2 Level, EUMETSAT, Darmstadt, Germany, EUM/OPS/EPS/DOC/12/0760, 150 pp., 2013.

EUMETSAT: GOME-2 Factsheet, EUMETSAT, Darmstadt, Germany, EUM/OPS/DOC/10/1299, v4b, 33 pp., 2014a.

EUMETSAT: GOME-2 L1 Product Generation Specification, EUMETSAT, Darmstadt, Germany, EPS.SYS.SPE.990011, v8, 462 pp., 2014b.

EUMETSAT: GOME-2/Metop-A PMD Band Definitions 3.0 and PMD Calibration, EUMETSAT, Darmstadt, Germany, EUM/OPS/EPS/DOC/12/0714, v1A, 15 pp., 2014c.

EUMETSAT: Generic Product Format Specification (GPFS), EUMETSAT, Darmstadt, Germany, EPS.GGS.SPE.96167, v8B, 72 pp., 2014d.

EUMETSAT: GOME-2 PPF6 AVHRR Cloud Properties - Validation Report, EUMETSAT, Darmstadt, Germany, EUM/TSS/DOC/14/763526, v1, 32 pp., 2014e.

EUMETSAT: Metop-A GOME Annual In-Flight Performance Review 2014, EUMETSAT, Darmstadt, Germany, EUM/OPS- EPS/REP/14/770718, v2A, 94 pp., 2015a.

EUMETSAT: Metop-B GOME Annual In-Flight Performance Review 2014, EUMETSAT, Darmstadt, Germany, EUM/OPS/EPS/REP/14/771772, v2A, 84 pp., 2015b.

Klaes, D., Cohen, M., Buhler, Y., Schlüssel, P., Munro, R., Luntama, J.-P., von Engeln, A., O’Clerigh, E., Bonekamp, H., Ackermann, J., and Schmetz, J.: An Introduction to the EUMETSAT Polar system, *B. Am. Meteorol. Soc.*, 88, 1085–1096, doi:10.1175/BAMS-88-7-1085, 2007.

Krijger, J. M., Snel, R., van Harten, G., Rietjens, J. H. H., and Aben, I.: Mirror contamination in space I: mirror modelling, *Atmos. Meas. Tech.*, 7, 3387–3398, doi:10.5194/amt-7-3387-2014, 2014.

Loyola, D. W. T., Livschitz, Y., Ruppert, T., Albert, P., and Hollmann, R.: Cloud properties derived from GOME/ERS-2 backscatter data for trace gas retrieval, *IEEE T. Geosci. Remote*, 45, 2747–2758, 2007.

Munro, R., Eisinger, M., Anderson, C., Callies, J., Corpaccioli, E., Lang, R., Lefebvre, A., Livschitz, Y., and Pérez Albiñana, A.: GOME-2 on MetOp, *Proc. of the 2006 EUMETSAT Meteorological Satellite Conference*, Helsinki, Finland, 12–16 June 2006, EUMETSAT, 8 pp., 2006.

The GOME-2 instrument on the Metop series of satellites

R. Munro et al.

Title Page

Abstract

Introduction

Conclusions

References

Tables

Figures

◀

▶

◀

▶

Back

Close

Full Screen / Esc

Printer-friendly Version

Interactive Discussion



Slijkhuis, S., Wahl, S., Aberle, B., and Loyola, D.: Re-analysis of GOME/ERS-2 Diffuser properties, in: Proceedings of the 2004 Envisat and ERS Symposium, Salzburg, Austria, SP-572 European Space Agency, 2P03-25, 2005.

Tilstra, L. G.: GOME-2 Polarisation Study Final Report, Netherlands Institute for Space Research, Utrecht, the Netherlands, SRON-EOS-RP-08-033, Issue 5 0.3, 2008.

Tilstra, L. G., Lang, R., Munro, R., Aben, I., and Stammes, P.: Contiguous polarisation spectra of the Earth from 300 to 850 nm measured by GOME-2 onboard MetOp-A, Atmos. Meas. Tech., 7, 2047–2059, doi:10.5194/amt-7-2047-2014, 2014.

TNO Space Systems Engineering: GOME-2 Calibration: Data Analysis Procedures, TNO Space Systems Engineering, Delft, the Netherlands, MO-RS-TPD-GO-0027, Issue 4, 69 pp., 2011a.

TNO Space Systems Engineering: GOME2 Calibration: Key Data File Structure Specification, TNO Space Systems Engineering, Delft, the Netherlands, MO-RS-TPD-GO-0025, Issue 6, 6 pp., 2011b.

TNO Space Systems Engineering: GOME-2 Instrument Calibration: Key Data Status List, TNO Space Systems Engineering, Delft, the Netherlands, MO-LI-TPD-GO-0037, Issue 5, 14 pp., 2012.

TPD Space Instrumentation: GOME-2 Calibration Error Budget, TNO Space Systems Engineering, Delft, the Netherlands, MO-RS-TPD-GO-0016, Issue 5, 31 pp., 2003.

TPD Space Instrumentation: GOME-2 Calibration Plan, TNO Space Systems Engineering, Delft, the Netherlands, MO-PL-TPD-GO-0004, Issue 5, 42 pp., 2004a.

TPD Space Instrumentation: GOME-2 FM3 Slit Function Test Report, TNO Space Systems Engineering, Delft, the Netherlands, MO-TR-TPD-GO-0101, Issue 2, 40 pp., 2004b.

Tuinder, O., Wang, P. and Stammes, P.: Support for Upgrade to FRESCO+ in the GOME-2 PPF: Final Report, EUM/CO/09/460000655/RM, Koninklijk Nederlands Meteorologisch Instituut, De Bilt, the Netherlands, 2011.

Wang, P., Stammes, P., van der A, R., Pinardi, G., and van Roozendael, M.: FRESCO+: an improved O₂ A-band cloud retrieval algorithm for tropospheric trace gas retrievals, Atmos. Chem. Phys., 8, 6565–6576, doi:10.5194/acp-8-6565-2008, 2008.

The GOME-2 instrument on the Metop series of satellites

R. Munro et al.

Title Page

Abstract

Introduction

Conclusions

References

Tables

Figures



Back

Close

Full Screen / Esc

Printer-friendly Version

Interactive Discussion



Table 1. Main GOME-2 instrument characteristics.

Wavelength Range	240–790 nm in 4 channels 300–800 nm in 2 polarisation detectors measuring polarisation perpendicular to and parallel to the instrument slit with 15 programmable spectral bands
Spectral Sampling	0.12–0.21 nm (main science channels)
Spectral Resolution	FWHM 0.26–0.51 nm (main science channels)
Orbit	Sun-synchronous, at an altitude of ~ 820 km, with a descending node equator crossing local solar time of 9:30
Swath Width	Default 1920 km
Spatial Resolution	Default 80 km across-track \times 40 km along-track (main science channels)
Data Rate	400 kbits s ⁻¹ or 300 MB (orbit) ⁻¹ (level 0 data) and ~ 800 MB (orbit) ⁻¹ (level 1)

The GOME-2 instrument on the Metop series of satellites

R. Munro et al.

Title Page

Abstract

Introduction

Conclusions

References

Tables

Figures



Back

Close

Full Screen / Esc

Printer-friendly Version

Interactive Discussion



Table 2. GOME-2 spectral coverage and resolution.

Channel	Approx. Spectral Range Metop-A [nm]	Approx. Spectral Range Metop-B [nm]	Detector Pixel Size [nm]	FWHM Metop-A [nm]	FWHM Metop-B [nm]
1	240–314	239–312	0.1	0.26	0.29
2	310–403	308–402	0.1	0.27	0.28
3	397–604	395–604	0.2	0.51	0.55
4	593–790	593–791	0.2	0.48	0.50
PMD-P					
PMD-S	312–790	312–790	0.62–8.8	2.9–37	2.9–37

The GOME-2 instrument on the Metop series of satellites

R. Munro et al.

Title Page

Abstract

Introduction

Conclusions

References

Tables

Figures

◀

▶

◀

▶

Back

Close

Full Screen / Esc

Printer-friendly Version

Interactive Discussion



Table 3. Main channel band settings of GOME-2. The band separation change between band 1A and B occurred for GOME-2 on Metop-A during orbit 11 119 on 10 December 2008. For GOME-2 on Metop-B the updated settings have been used from the beginning of operations.

Channel	Band	Number of Pixels	Approximate Spectral Range (nm) Metop-A	Approximate Spectral Range (nm) Metop-B	nm pixel ⁻¹
1	1A	877/659 *	240–307/283 ¹	239–283	0.07
1	1B	147/365	307/283–314 ¹	283–312	0.07
2	2A	71	not valid	not valid	0.09
2	2B	953	310–403	308–402	0.09
3	3	1024	397–604	395–604	0.2
4	4	1024	593–790	593–791	0.2
5/6	PMD P/S	256	312–790	312–790	2

* Settings changed on 10 December 2008.

The GOME-2 instrument on the Metop series of satellites

R. Munro et al.

Title Page

Abstract

Introduction

Conclusions

References

Tables

Figures

◀

▶

◀

▶

Back

Close

Full Screen / Esc

Printer-friendly Version

Interactive Discussion



Table 4. Default GOME-2 Metop-A PMD band definitions (v1.0) valid from date of launch to 11 March 2008 in orbit 7226.

Band	First Pixel from Start of Block-C	Number of Pixels	Approx. Start Wavelength [nm]	Approx. End Wavelength [nm]
0	19	2	309.2	309.9
1	23	5	311.7	314.4
2	31	4	317.0	319.1
3	37	12	321.2	329.5
4	50	5	331.1	334.3
5	56	43	335.9	377.7
6	100	4	380.1	383.7
7	115	20	399.3	428.4
8	138	43	435.5	552.5
9	183	2	553.6	557.5
10	187	22	569.6	678.6
11	217	2	742.3	750.2
12	219	1	758.2	758.2
13	223	1	792.1	792.1
14	228	1	838.8	838.8

The GOME-2 instrument on the Metop series of satellites

R. Munro et al.

[Title Page](#)
[Abstract](#)
[Introduction](#)
[Conclusions](#)
[References](#)
[Tables](#)
[Figures](#)
[◀](#)
[▶](#)
[◀](#)
[▶](#)
[Back](#)
[Close](#)
[Full Screen / Esc](#)
[Printer-friendly Version](#)
[Interactive Discussion](#)


Table 6. GOME-2 Metop-B PMD band definitions (v2.0). This set is valid from 29 October 2012 during orbit 598. Here “P” indicates PMD-P which measures intensity polarised parallel to the spectrometer’s slit, and “S” indicates PMD-S which measures intensity polarised perpendicular to the spectrometer’s slit.

Band	First Pixel from Start of Block-C		Number of Pixels		Approx. Start Wavelength [nm]		Approx. End Wavelength [nm]	
	S	P	S	P	S	P	S	P
0	22	23	5	5	311.875	312.001	314.375	314.516
1	30	31	4	4	316.948	317.102	318.926	319.090
2	37	38	12	12	321.634	321.807	329.514	329.675
3	50	51	6	6	331.016	331.172	334.872	335.020
4	56	57	6	6	335.661	335.808	339.698	339.848
5	84	85	17	17	360.644	360.825	378.138	378.308
6	102	103	4	4	380.515	380.706	384.170	384.399
7	117	118	19	19	400.059	400.383	428.350	428.763
8	139	140	27	27	435.521	435.971	493.181	493.963
9	166	167	18	18	495.886	496.683	549.510	550.625
10	184	185	2	2	553.192	554.330	556.944	558.106
11	188	189	11	11	568.637	569.885	612.854	614.699
12	199	200	8	8	617.781	619.714	656.047	658.343
13	218	219	4	4	737.179	739.726	760.682	763.366
14	224	225	2	2	785.719	788.551	794.415	797.300

The GOME-2 instrument on the Metop series of satellites

R. Munro et al.

Title Page

Abstract

Introduction

Conclusions

References

Tables

Figures



Back

Close

Full Screen / Esc

Printer-friendly Version

Interactive Discussion



Table 7. Validity region of the etalon correction.

Channel Number	Detector Pixel Start/Stop	Approximate Wavelength Start/Stop [nm]
1	310/935	243.4/312.8
2	210/850	316.5/392.1
3	120/1009	417.1/604.1
4	85/989	603.2/790.8
PMD-P	750/997	299.9/842.3
PMD-S	750/998	299.9/852.3

The GOME-2 instrument on the Metop series of satellites

R. Munro et al.

Title Page

Abstract Introduction

Conclusions References

Tables Figures

◀ ▶

◀ ▶

Back Close

Full Screen / Esc

Printer-friendly Version

Interactive Discussion



GOME-2/Metop-A timeline planning per 412/29 repeat cycle. Version 5.0, July 2013 - Start of Tandem Operations

day	orbit offset	1	2	3	4	5	6	7	8	9	10	11	12	13	14	15
1	0	X	X	X	M1	M2	D1	D2	X	X	S	S	R	X	X	X
2	15	X	X	X	X	X	D1	D2	X	X	X	X	X	X	X	X
3	29	X	X	X	X	X	D1	D2	X	X	X	X	X	X	X	X
4	43	X	X	X	X	X	D1	D2	X	X	X	X	X	X	X	X
5	57	X	X	X	X	X	D1	D2	X	X	X	X	X	X	X	X
6	72	X	X	X	X	X	D1	D2	X	X	X	X	X	X	X	X
7	86	X	X	X	X	X	D1	D2	X	X	X	X	X	X	X	X
8	100	X	X	X	X	X	D1	D2	X	X	X	X	X	X	X	X
9	114	X	X	X	X	X	D1	D2	X	X	X	X	X	X	X	X
10	128	X	X	X	X	X	D1	D2	X	X	X	X	X	X	X	X
11	143	X	X	X	X	X	D1	D2	X	X	X	X	X	X	X	X
12	157	X	X	X	X	X	D1	D2	X	X	X	X	X	X	X	X
13	171	X	X	X	X	X	D1	D2	X	X	X	X	X	X	X	X
14	185	X	X	X	X	X	D1	D2	X	X	X	X	X	X	X	X
15	199	N3	N3	N3	N3	N3	D1	D2	N3							
16	214	X	X	X	X	X	D1	D2	X	X	X	X	X	X	X	X
17	228	X	X	X	X	X	D1	D2	X	X	X	X	X	X	X	X
18	242	X	X	X	X	X	D1	D2	X	X	X	X	X	X	X	X
19	256	X	X	X	X	X	D1	D2	X	X	X	X	X	X	X	X
20	270	X	X	X	X	X	D1	D2	X	X	X	X	X	X	X	X
21	285	X	X	X	X	X	D1	D2	X	X	X	X	X	X	X	X
22	299	X	X	X	X	X	D1	D2	X	X	X	X	X	X	X	X
23	313	X	X	X	X	X	D1	D2	X	X	X	X	X	X	X	X
24	327	X	X	X	X	X	D1	D2	X	X	X	X	X	X	X	X
25	341	X	X	X	X	X	D1	D2	X	X	X	X	X	X	X	X
26	356	X	X	X	X	X	D1	D2	X	X	X	X	X	X	X	X
27	370	X	X	X	X	X	D1	D2	X	X	X	X	X	X	X	X
28	384	X	X	X	X	X	D1	D2	X	X	X	X	X	X	X	X
29	398	X	X	X	X	X	D1	D2	X	X	X	X	X	X	X	X

D1	CALNS6	Daily calibration, part 1 (SLS/WLS) with 960 km swath
D2	CALNS0	Daily calibration, part 2 (Sun) with 960 km swath
M1	CALNS4	Monthly calibration, part 1 (LED, WLS, SLS modes) with 960 km swath
M2	CALNS5	Monthly calibration, part 2 (SLS over diffuser mode) with 960 km swath
N3	NOT320	Narrow swath (320 km)
S	NADIR	Nadir static
R	PMDRAWNS	PMD monitoring (nominal readout/raw transfer mode) with 960 km swath
X	NOT960	Nominal swath (960 km)

Figure 2. The 29 day instrument operation cycle for GOME-2 on Metop-A. Different colours and ID tags indicate different instrument operations settings as explained in the legend.

The GOME-2 instrument on the Metop series of satellites

R. Munro et al.

[Title Page](#)

[Abstract](#) [Introduction](#)

[Conclusions](#) [References](#)

[Tables](#) [Figures](#)

[◀](#) [▶](#)

[◀](#) [▶](#)

[Back](#) [Close](#)

[Full Screen / Esc](#)

[Printer-friendly Version](#)

[Interactive Discussion](#)

GOME-2/Metop-B timeline planning per 412/29 repeat cycle. Version 1.0, July 2013 - Start of Tandem Operations

day	orbit offset	1	2	3	4	5	6	7	8	9	10	11	12	13	14	15
1	0	X	X	X	M1	M2	D1	D2	X	X	S	S	R	X	X	X
2	15	X	X	X	X	X	D1	D2	X	X	X	X	X	X	X	
3	29	X	X	X	X	X	D1	D2	X	X	X	X	X	X	X	
4	43	X	X	X	X	X	D1	D2	X	X	X	X	X	X	X	
5	57	X	X	X	X	X	D1	D2	X	X	X	X	X	X	X	X
6	72	X	X	X	X	X	D1	D2	X	X	X	X	X	X	X	
7	86	X	X	X	X	X	D1	D2	X	X	X	X	X	X	X	
8	100	X	X	X	X	X	D1	D2	X	X	X	X	X	X	X	
9	114	X	X	X	X	X	D1	D2	X	X	X	X	X	X	X	
10	128	X	X	X	X	X	D1	D2	X	X	X	X	X	X	X	X
11	143	X	X	X	X	X	D1	D2	X	X	X	X	X	X	X	X
12	157	X	X	X	X	X	D1	D2	X	X	X	X	X	X	X	
13	171	X	X	X	X	X	D1	D2	X	X	X	X	X	X	X	
14	185	X	X	X	X	X	D1	D2	X	X	X	X	X	X	X	
15	199	X	X	X	X	X	D1	D2	X	X	X	X	X	X	X	X
16	214	X	X	X	X	X	D1	D2	X	X	X	X	X	X	X	X
17	228	X	X	X	X	X	D1	D2	X	X	X	X	X	X	X	
18	242	X	X	X	X	X	D1	D2	X	X	X	X	X	X	X	
19	256	X	X	X	X	X	D1	D2	X	X	X	X	X	X	X	
20	270	X	X	X	X	X	D1	D2	X	X	X	X	X	X	X	X
21	285	X	X	X	X	X	D1	D2	X	X	X	X	X	X	X	X
22	299	X	X	X	X	X	D1	D2	X	X	X	X	X	X	X	X
23	313	X	X	X	X	X	D1	D2	X	X	X	X	X	X	X	
24	327	X	X	X	X	X	D1	D2	X	X	X	X	X	X	X	
25	341	X	X	X	X	X	D1	D2	X	X	X	X	X	X	X	X
26	356	X	X	X	X	X	D1	D2	X	X	X	X	X	X	X	
27	370	X	X	X	X	X	D1	D2	X	X	X	X	X	X	X	
28	384	X	X	X	X	X	D1	D2	X	X	X	X	X	X	X	
29	398	X	X	X	X	X	D1	D2	X	X	X	X	X	X	X	

D1	CAL6	Daily calibration, part 1 (SLS/WLS) with 1920 km swath
D2	CAL0	Daily calibration, part 2 (Sun) with 1920 km swath
M1	CAL4	Monthly calibration, part 1 (LED, WLS, SLS modes) with 1920 km swath
M2	CAL5	Monthly calibration, part 2 (SLS over diffuser mode) with 1920 km swath
S	NADIR	Nadir static
R	PMDRAW	PMD monitoring (nominal readout/raw transfer mode) with 1920 km swath
X	NOT1920	Nominal swath (1920 km)

Figure 3. The 29 day instrument operation cycle of GOME-2 on Metop-B. Different colours and ID tags indicate different instrument operations settings as explained in the legend.



The GOME-2 instrument on the Metop series of satellites

R. Munro et al.

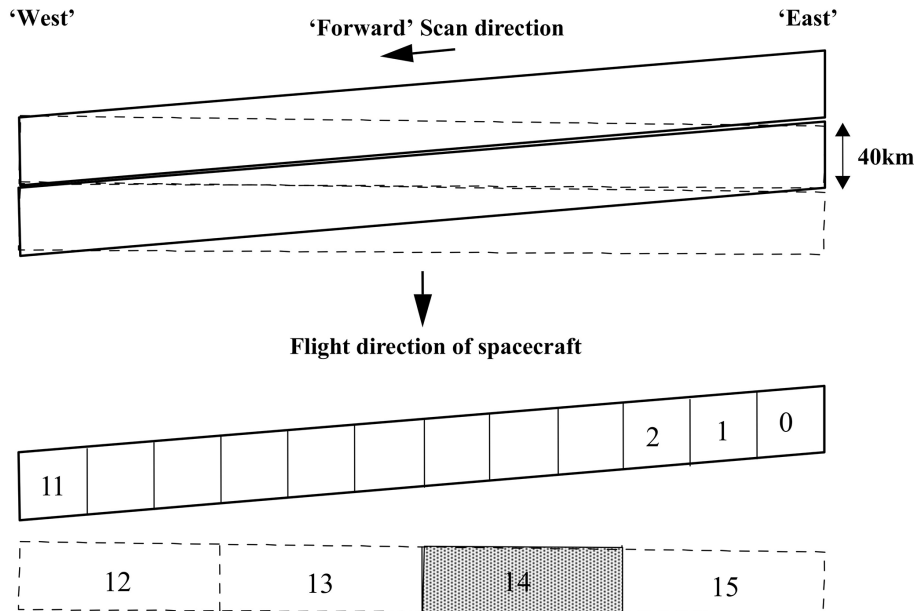


Figure 4. Scan pattern in default scan mode. Solid line: forward scan; dashed line: fly back. Each subset pixel (0–15) corresponds to 375 ms. In one of the four subsets of the fly back (subset 14 is shown as an example only) the “unused” parts of the PMD detectors (i.e. Block A see Appendix B of EUMETSAT, 2014a) are read out.

Title Page

Abstract Introduction

Conclusions References

Tables Figures

◀ ▶

◀ ▶

Back Close

Full Screen / Esc

Printer-friendly Version

Interactive Discussion



The GOME-2 instrument on the Metop series of satellites

R. Munro et al.

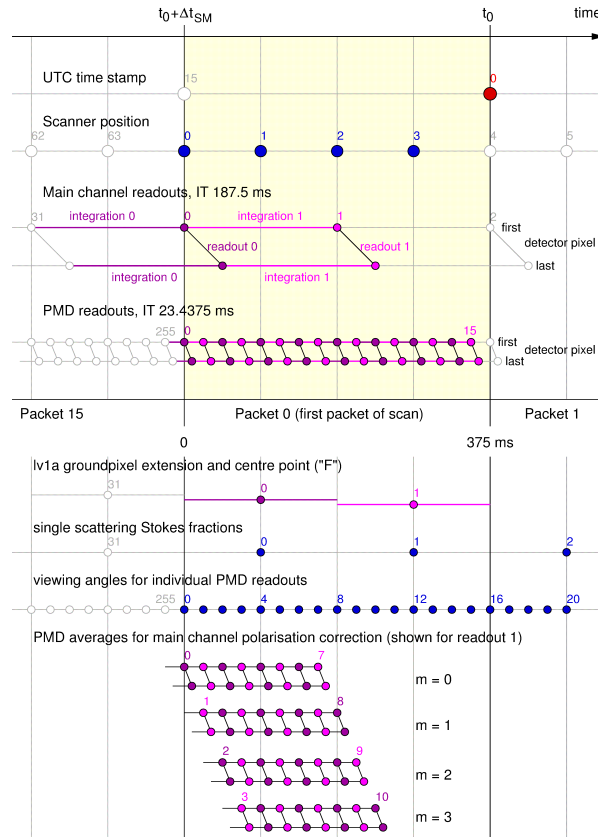


Figure 5. Synchronisation diagram. Synchronisation of time stamp, scanner positions and detector readouts within a GOME-2 science data packet, and selected quantities of the level 0 to 1a processing. The data transmitted in packet 0 (the first of a scan) is indicated by the filled circles. Open circles belong to the previous or next data packet. For this figure, Δt_{SM} was assumed to be -375 ms. The indexing refers to a complete scan.

Title Page

Abstract

Introduction

Conclusions

References

Tables

Figures

◀

▶

◀

▶

Back

Close

Full Screen / Esc

Printer-friendly Version

Interactive Discussion



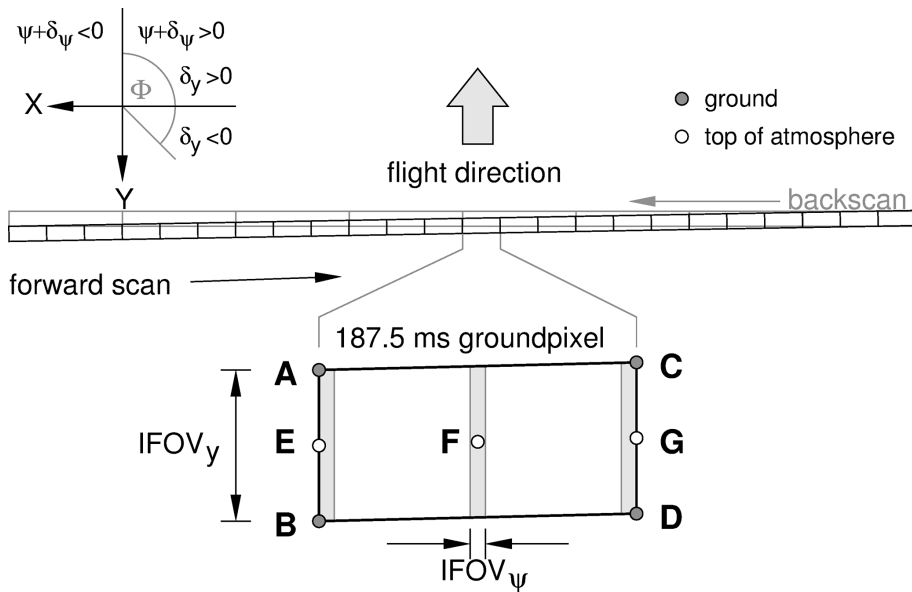


Figure 6. GOME-2 ground pixel orientation relative to the scan and the flight direction.

The GOME-2 instrument on the Metop series of satellites

R. Munro et al.

Title Page	
Abstract	Introduction
Conclusions	References
Tables	Figures
◀	▶
◀	▶
Back	Close
Full Screen / Esc	
Printer-friendly Version	
Interactive Discussion	



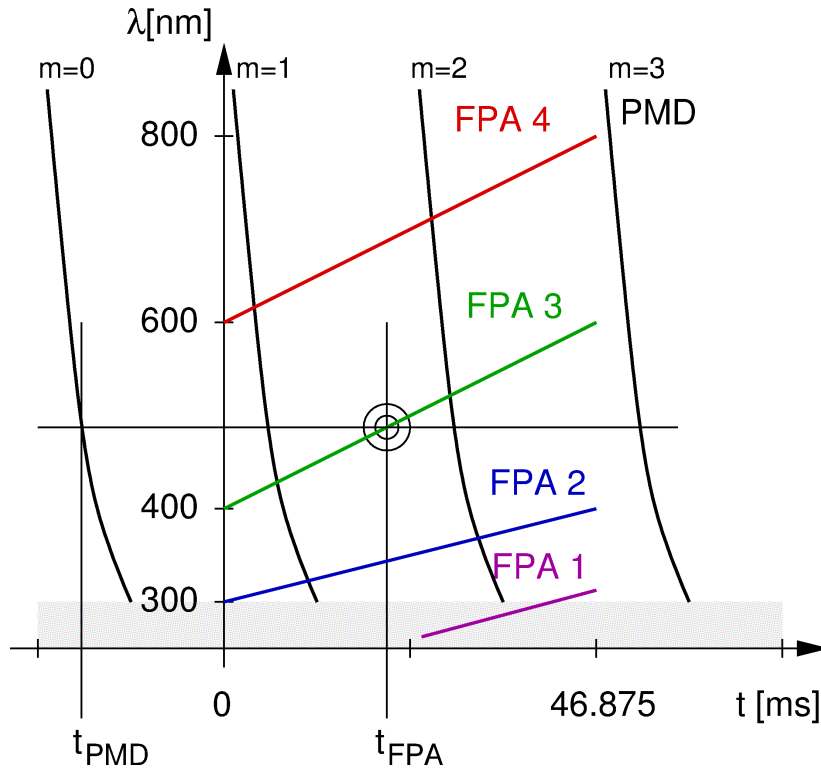


Figure 7. Timing diagram for main channel and PMD detector pixel readouts. For this example, readout sequence “up” has been assumed for the four main channels, and readout sequence “down” for the two PMD channels. Readout of the main channels and readout of the PMD channels for $m = 1$ starts at $t = 0$. For a given detector pixel in a main channel, indicated by the circles, its readout time t_{FPA} and the one of the PMD-Pixel closest in wavelength, t_{PMD} are determined. The difference between the two times is then used for linear interpolation of the PMD data between the two adjacent PMD curves.

The GOME-2 instrument on the Metop series of satellites

R. Munro et al.

Title Page

Abstract Introduction

Conclusions References

Tables Figures

◀ ▶

◀ ▶

Back Close

Full Screen / Esc

Printer-friendly Version

Interactive Discussion



The GOME-2 instrument on the Metop series of satellites

R. Munro et al.

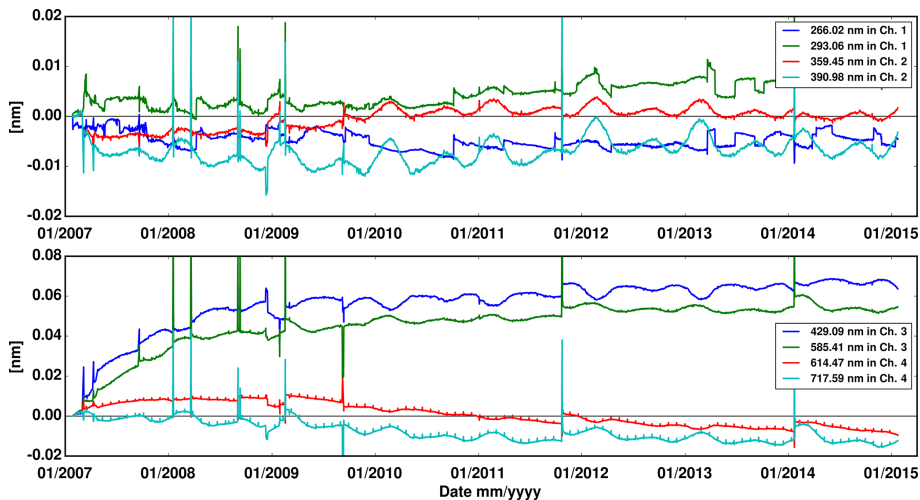


Figure 8. Difference of the centre line position with respect to January 2007 evaluated from a regular Gaussian fitting of well separated SLS lines. Upper panel shows the results in channel 1 and 2. The lower panel results for channel 3 and 4.

Title Page

Abstract

Introduction

Conclusions

References

Tables

Figures



Back

Close

Full Screen / Esc

Printer-friendly Version

Interactive Discussion



**The GOME-2
instrument on the
Metop series of
satellites**

R. Munro et al.

Title Page

Abstract

Introduction

Conclusions

References

Tables

Figures

◀

▶

◀

▶

Back

Close

Full Screen / Esc

Printer-friendly Version

Interactive Discussion

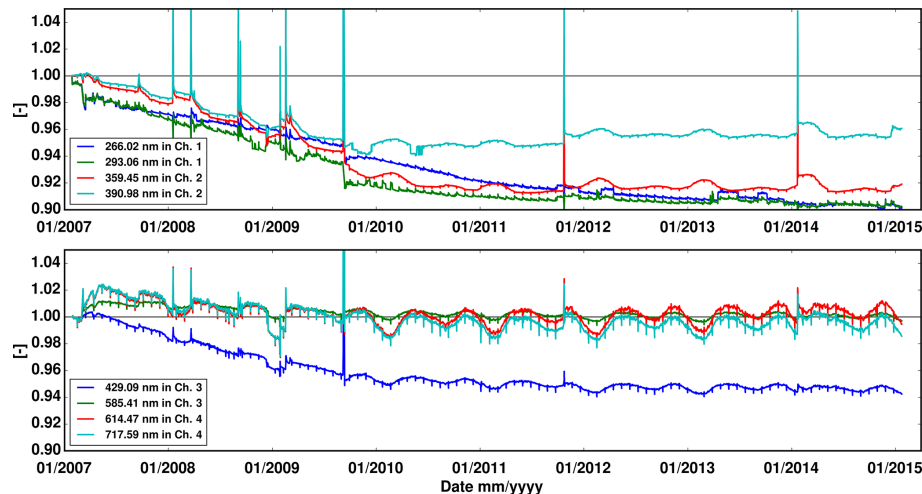


Figure 9. FWHM relative change with respect to January 2007 evaluated from a regular Gaussian fitting of well separated SLS lines. Upper panel shows the results in channel 1 and 2. The lower panel results for channel 3 and 4.

**The GOME-2
instrument on the
Metop series of
satellites**

R. Munro et al.

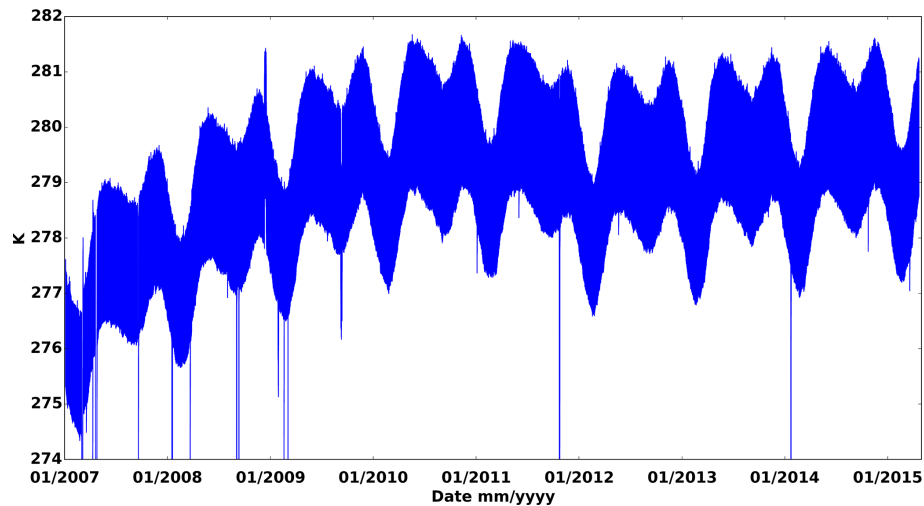
[Title Page](#)[Abstract](#)[Introduction](#)[Conclusions](#)[References](#)[Tables](#)[Figures](#)[Back](#)[Close](#)[Full Screen / Esc](#)[Printer-friendly Version](#)[Interactive Discussion](#)

Figure 10. Instrument Optical bench temperature. The orbital variation is about 1 K.

The GOME-2 instrument on the Metop series of satellites

R. Munro et al.

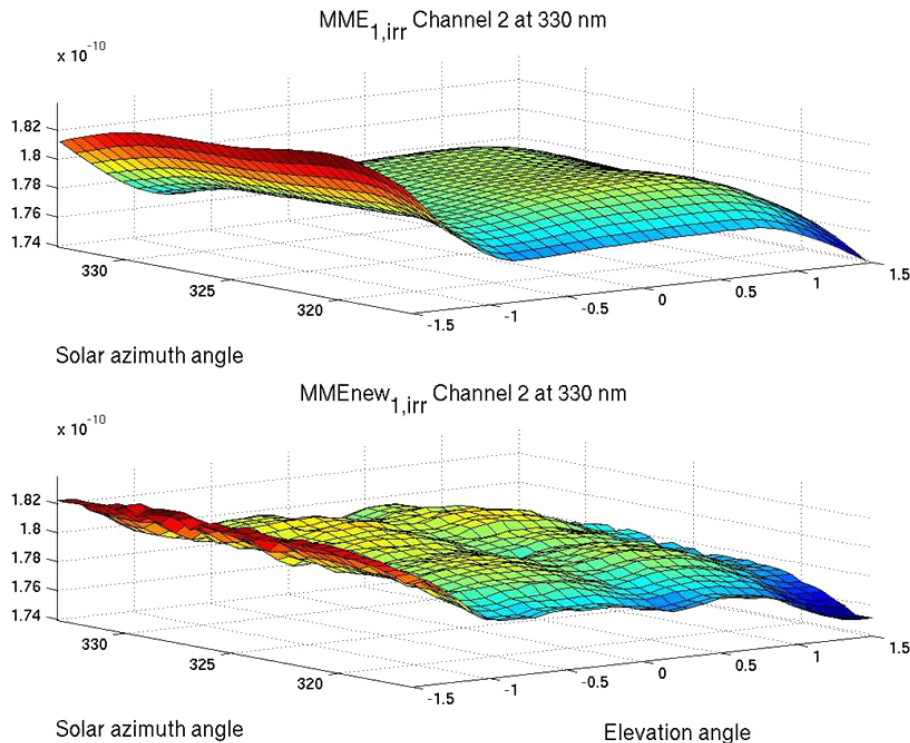


Figure 11. Mueller Matrix elements (MMEs) at 330 nm for the radiometric calibration of the irradiance signals including the dependence on elevation and solar azimuth angles. The irradiance response MMEs consist of the diffuser BSDF and the radiometric response per channel. The top panel shows the MME as derived from the on-ground characterisation and the lower panel the same but derived from in-flight data.

Title Page

Abstract

Introduction

Conclusions

References

Tables

Figures

◀

▶

◀

▶

Back

Close

Full Screen / Esc

Printer-friendly Version

Interactive Discussion



The GOME-2 instrument on the Metop series of satellites

R. Munro et al.

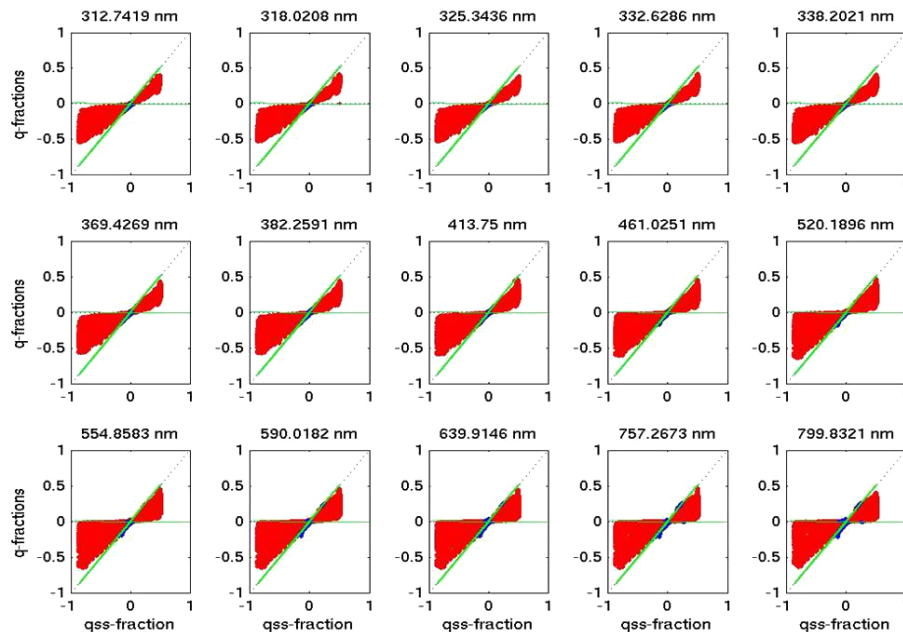


Figure 12. Limiting atmosphere plot for Earthshine q Stokes fractions and for all PMD bands. The data is derived from one orbit on 31 July 2009. The green lines indicate the Rayleigh single scattering values and $q = 0$. Red points lie inside the physically reasonable range while blue points lie outside the physically reasonable range.

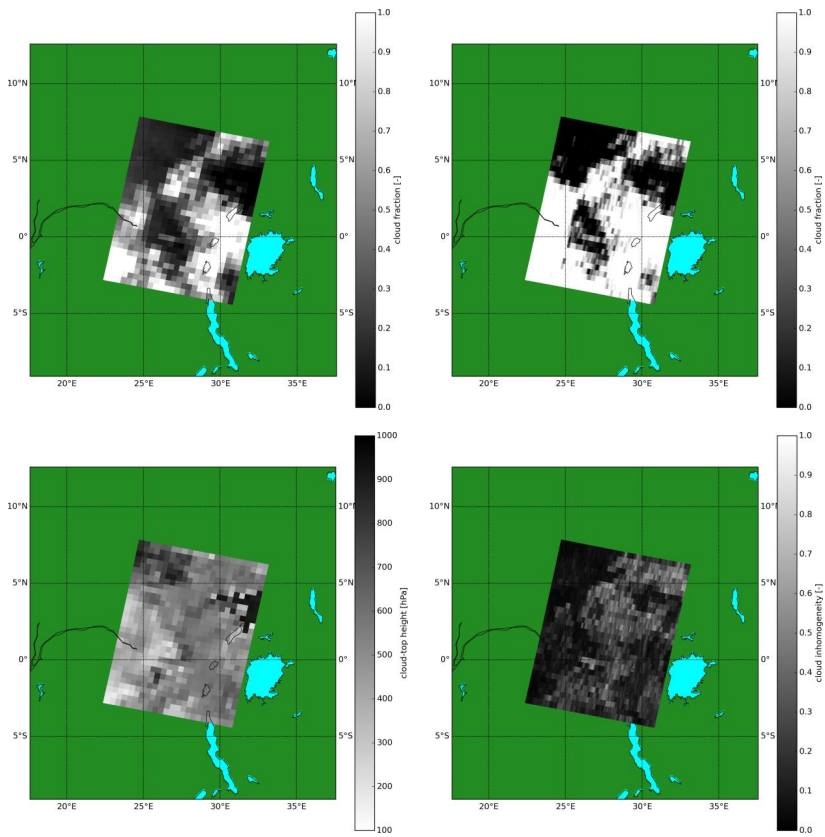


Figure 13. FRESCO+ cloud fraction (upper left panel) and the AVHRR derived cloud fraction (upper right panel) for sample data for GOME-2 Metop-A from March 2015. Also shown are the FRESCO+ cloud top height (lower left panel) and the AVHRR derived inhomogeneity (lower right panel).

The GOME-2 instrument on the Metop series of satellites

R. Munro et al.

Title Page

Abstract

Introduction

Conclusions

References

Tables

Figures

◀

▶

◀

▶

Back

Close

Full Screen / Esc

Printer-friendly Version

Interactive Discussion



The GOME-2 instrument on the Metop series of satellites

R. Munro et al.

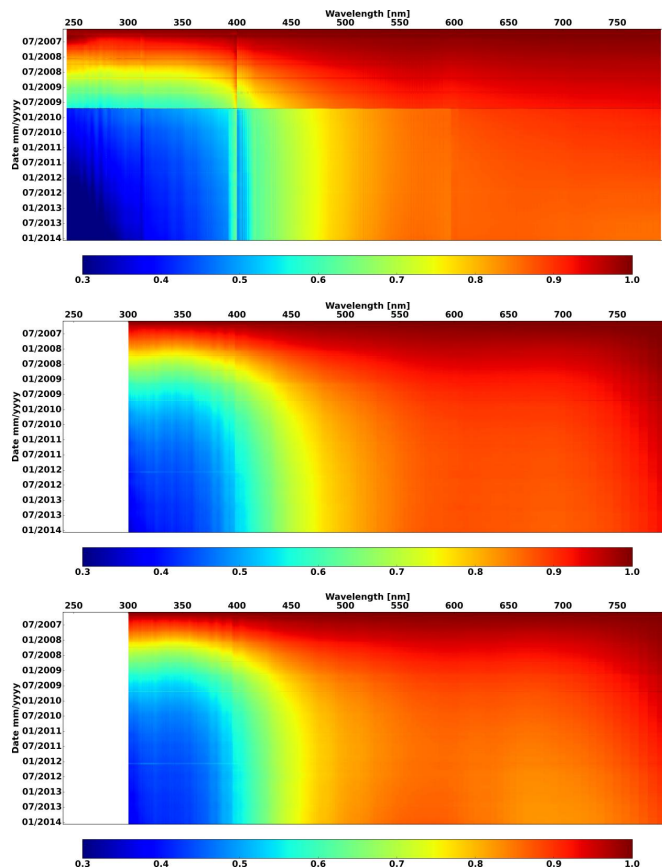


Figure 14. SMR spectra for all four main channels (upper panel), PMD-S (middle panel), and PMD-P (lower panel) normalised to January 2007. The discontinuity in the main channels in September 2009 is the second throughput test (EUMETSAT, 2011). The discontinuities in spectral space for the main channels are the channel overlap regions.

[Title Page](#)
[Abstract](#)
[Introduction](#)
[Conclusions](#)
[References](#)
[Tables](#)
[Figures](#)
[◀](#)
[▶](#)
[◀](#)
[▶](#)
[Back](#)
[Close](#)
[Full Screen / Esc](#)
[Printer-friendly Version](#)
[Interactive Discussion](#)
